Talanta 128 (2014) 327–336

Contents lists available at ScienceDirect

Talanta

journal homepage: www.elsevier.com/locate/talanta

Dual fluorescence resonance energy transfer assay between tunable upconversion nanoparticles and controlled gold nanoparticles for the simultaneous detection of Pb^{2+} and Hg^{2+}

Shijia Wu, Nuo Duan, Zhao Shi, Congcong Fang, Zhouping Wang*

State Key Laboratory of Food Science and Technology, Synergetic Innovation Center of Food Safety and Nutrition, School of Food Science and Technology, Jiangnan University, Wuxi 214122, PR China

ARTICLE INFO

Article history:
Received 27 January 2014
Received in revised form
16 April 2014
Accepted 21 April 2014
Available online 30 April 2014

Keywords:
Upconversion nanoparticles
Gold nanoparticles
Aptamer
Pb^{2+} and Hg^{2+}

ABSTRACT

In this work, we presented a novel dual fluorescence resonance energy transfer (FRET) system for the simultaneous detection of Pb^{2+} and Hg^{2+}. This system employed two color upconversion nanoparticles (UCNPs) as the donors, and controlled gold nanoparticles (AuNPs) as the acceptors. The two donor–acceptor pairs were fabricated by hybridizing the aptamers and their corresponding complementary DNA. Thus, the green and red upconversion fluorescence could be quenched because of a good overlap between the UCNPs fluorescence emission and the AuNPs absorption spectrum. In the presence of Pb^{2+} and Hg^{2+}, the aptamers preferred to bind to their corresponding analytes and formed a G-quadruplexes structure for Pb^{2+} and the hairpin-like structure for Hg^{2+}. As a result, the dual FRET was disrupted, and the green and red upconversion fluorescence was restored. Under optimized experimental conditions, the relative fluorescence intensity increased as the metal ion concentrations were increased, allowing for the quantification of Pb^{2+} and Hg^{2+}. The relationships between the fluorescence intensity and plotting logarithms of ion concentrations were linear in the range from 0.1 to 100 nM for Pb^{2+} and 0.5 to 500 nM for Hg^{2+}, and the detection limits of Pb^{2+} and Hg^{2+} were 50 pM and 150 pM, respectively. As a practical application, the aptasensor was used to monitor Pb^{2+} and Hg^{2+} levels in naturally contaminated samples and human serum samples. Ultimately, this type of dual FRET could be used to detect other metal ions or contaminants in food safety analysis and environment monitoring.

1. Introduction

Heavy metal contamination constitutes a global environmental hazard due to its highly bioaccumulation, non-biodegradability property and high toxicity. Particularly, lead and mercury are two of the most toxic metallic pollutants; they can damage various systems in the body. Although inductively coupled plasma mass spectrometry (ICP-MS) [1–4], atomic absorption spectrum (AAS) [5–7] and high performance liquid chromatography (HPLC) [8], the powerful techniques, are used in most current protocols for the detecting these two metal ions, it is rather expensive, sophisticated, and unsuitable for fast detection and on-site analyses. On the other hand, electrochemical [9–14] and sensing techniques [15,16] have well performance in real samples. Recently, detection systems using fluorescence and DNA have become popular, mainly because fluorescence is sensitive and DNA is stable and a specific binder of certain targets. However, few reports about fluorescence methods and DNA-based methods are applied in simultaneous detection of Pb^{2+} and Hg^{2+}, they are generally limited to the detection of only one of two metal ions [17,18]. For example, Chang and coworkers reported that a thrombin-binding aptamer (TBA) probe could bind Pb^{2+} and Hg^{2+} ions individually [19]. Chung and coworkers also built an aptasensor for the detection of Pb^{2+} and Hg^{2+} in human serum. Two fluorophores were used as the donors for monitoring Pb^{2+} and Hg^{2+} [20]. However, the excitation wavelengths of the two fluorophores were different. Therefore, it is of great interest and necessary to develop an analytical method based on fluorescence coupled with DNA that can simultaneously detect coexisting lead and mercury in food and the environment.

In recent years, there has been considerable interest in rare-earth upconversion nanoparticles (UCNPs) that are doped with lanthanide ions. UCNPs exhibit unique luminescence properties, including the ability to convert longer wavelength radiation to shorter wavelength fluorescence via a two-photon or multi-photon mechanism [21,22]. Therefore, UCNPs are promising candidates for the analysis of biological and environmental samples and are widely used as novel

* Corresponding author. Tel./fax: +86 510 85917023.
E-mail address: wangzp@jiangnan.edu.cn (Z. Wang).

http://dx.doi.org/10.1016/j.talanta.2014.04.056
0039-9140/

fluorescence labels [23–28]. UCNPs have also attracted considerable interest because their optical properties can be tuned by varying the lanthanide dopant such as Er^{3+}, Tm^{3+} and Ho^{3+}. Because of their tunable, multicolor emissions in the visible spectral region, they can be extensively employed in bioimaging in vivo and in vitro [29–31]. However, few reports have focused on developing UCNPs as multicolor labels for simultaneous quantitative analysis. Some multicolor UCNPs-based biosensors were built successfully by our group [32–34]. This work helped us to develop the novel biosensors for the simultaneous detection of various analytes.

Both spherical shaped and rod-like shaped gold nanoparticles have attracted considerable attention because they can be used in the chemical and biochemical sensing applications. In fact, the size- and shape-controlled synthesis of gold nanoparticles is important for current advanced materials because nearly every property, including the optical, catalytic and surface activities, is size- and shape-dependent within the nanometer regime [35]. Spherical and rod-shaped gold nanoparticles exhibit different surface plasmon resonance (SPR). The UV–vis spectra of gold nanorods exhibits two SPR peaks, in particular, a longitudinal surface plasmon resonance (LSPR) peak, while gold nanoballs have a single SPR. Due to their strong SPR absorption, they can be employed as good quenching effect acceptors. Moreover, the distinct difference SPR absorbance bands of gold nanoballs and gold nanorods can be potentially applied in multiplexed fluorescence resonance energy transfer (FRET). To date, either UCNPs binding to gold nanoballs [23,36] or UCNPs binding with gold nanorods [37,38] have been used as single donor–acceptor pairs to build FRET systems. Matching the tunable, multicolor UCNPs emission peaks to the controlled SPR peaks of gold nanoparticles to create several donor–acceptor pairs in a single FRET system is a more valuable research direction.

Herein, $NaYF_4$: Yb, Ho UCNPs and Mn^{2+}-doped $NaYF_4$: Yb, Er UCNPs which excited by a 980 nm laser were employed as donors. As a potential alternative, gold nanoballs and gold nanorods were chosen as the acceptors for the corresponding donors because of their good quenching abilities and specific absorption. Thus, a homogenous dual FRET system was fabricated between two donor–acceptor pairs to detect Pb^{2+} and Hg^{2+} simultaneously. The method presented here is highly sensitive and selective due to the near-infrared laser-induced upconversion fluorescence without autofluorescence interference and the high specificity of the aptamers. More importantly, no earlier reports of using two colors UCNPs as donors and two different AuNPs SPR peaks as acceptors in a homogenous system have appeared in the literature.

2. Materials and methods

2.1. Chemicals

The rare-earth nitrates used in this work, including $Y(NO_3)_3 \cdot 6H_2O$, $Yb(NO_3)_3 \cdot 5H_2O$, $Ho(NO_3)_3 \cdot 5H_2O$ and $Er(NO_3)_3 \cdot 5H_2O$ were of 99.99% pure and purchased from Aladdin Industrial Inc. (Shanghai, China). $Hg(NO_3)_2$, $Pb(NO_3)_2$, $MnCl_2$, NaF, NaOH, HCl, $NaBH_4$, $AgNO_3$, toluene, cyclohexane, ethanol and $HAuCl_4 \cdot 3H_2O$, and ascorbic acid were of analytical grade. All these chemicals were purchased from Sinopharm Chemical Reagent Co., Ltd. (Shanghai, China). 1-Ethyl-3-(3-dimethylaminopropyl)carbodiimide hydrochloride (EDC), N-hydroxysulfosuccinimide sodium salt (sulfo-NHS), poly(acrylic acid) (PAA), diethylene glycol (abbreviated as DEG) and oleic acid were obtained from Sigma-Aldrich (U.S.A.). The sequences of the Pb^{2+} aptamer and the Hg^{2+} aptamers and the complementary DNA of the Pb^{2+} aptamers and the complementary DNA of the Hg^{2+} aptamers (in Table 1) were synthesized by Sangon Biotechnology Co., Ltd. (Shanghai, China).

Table 1
The sequences of the Pb^{2+} aptamers and the Hg^{2+} aptamer and the complementary DNA of the Pb^{2+} aptamer and Hg^{2+} aptamers.

Sample name	Abbreviation	Sequence (5′-3′)
Pb^{2+} aptamer	Apt_1	NH_2-GGGTGGGTGGGTGGGT
Hg^{2+} aptamer	Apt_2	NH_2-TCATCGTTCTTTCTTCCC-CTTGTTTGTT
complementary DNA of the Pb^{2+} aptamer	$cDNA_1$	SH-CACCCTCCCAC
complementary DNA of the Hg^{2+} aptamer	$cDNA_2$	SH-AGAACGATGA

2.2. Instruments

The size and morphology of the nanoparticles were determined using a JEM-2100HR transmission electron microscope (TEM, JEOL Ltd., Japan) at 200 kV. X-ray diffraction (XRD) measurements were performed using a D8-Advance instrument (Bruker AXS Ltd., Germany). Upconversion fluorescence spectra were measured using an F-7000 fluorescence spectrophotometer (Hitachi Co., Japan) modified with a 980 nm laser (Beijing Hi-Tech Optoelectronic Co., China) instead of a Xenon source. The zeta potential was measured using a Malvern Zetasizer Nano ZS90 apparatus (Malvern Instruments, United Kingdom). UV–visible absorption spectra were measured using an Evolution 260 Bio micro-spectrophotometer (Thermo Electron Co., U.S.A.). FT-IR spectra of the bionanoparticles were obtained with a Nicolet Nexus 470 Fourier transforms infrared spectrophotometer (Thermo Electron Co., U.S.A.).

2.3. Synthesis and surface modification of upconversion nanoparticles

Various oleic acid-capped UCNPs were prepared by a modified hydrothermal process [39,40]. In a typical $NaYF_4$: Yb, Ho UCNPs synthesis procedure, NaOH (1.2 g, 30 mmol), water (9 mL), ethanol (10 mL), and oleic acid (20 mL) were mixed under agitation to form a homogeneous solution. Then, 0.936 mL of 0.5 M $Y(NO_3)_3$, 0.6 mL of 0.2 M $Yb(NO_3)_3$ and 0.06 mL of 0.2 M $Ho(NO_3)_3$ (Y:Yb:Ho = 78 mol%: 20 mol%: 2 mol%) were added to the mixture, which was stirred thoroughly. Subsequently, 0.168 g of a NaF (4 mmol) solution was added dropwise to the above solution. After vigorously stirring at room temperature for 15 min, the colloidal solution was transferred into a 50 mL Teflon-lined autoclave, sealed and heated at 190 °C for 12 h. The system was allowed to cool to room temperature, and the products were deposited by adding ethanol to the bottom of the vessel. The resulting mixture was then centrifuged to obtain the powdered sample. The samples were purified with ethanol several times to remove oleic acid, sodium oleate and other remnants before drying under vacuum at 70 °C to obtain the dried $NaYF_4$: Yb, Ho UCNPs powder. The Mn^{2+} ions doped $NaYF_4$: Yb, Er UCNPs were synthesized in a similar manner by varying the amount of Mn^{2+} and the rare-earth elements. In brief, 0.6 mL of 0.5 M $MnCl_2$, 1 mL of 0.5 M $Y(NO_3)_3$, 0.9 mL of a 0.2 M $Yb(NO_3)_3$ and 0.1 mL of 0.2 M $Er(NO_3)_3$ aqueous solution were added under magnetic stirring. Finally, Mn^{2+}-doped $NaYF_4$: Yb, Er UCNPs were obtained.

The oleic acid-capped UCNPs can be well dispersed in nonpolar solvents including cyclohexane, chloroform and toluene. However, for biological labeling applications, UCNPs should be compatible with biomolecules such as nucleic acids and live cells. It was necessary to convert the hydrophobic UCNPs into hydrophilic ones. A slightly modified method for ligand exchange using PAA was employed [41]. Typically, PAA (0.5 g) was added to 10 mL of diethylene glycol (DEG), and the mixture was heated to 110 °C with vigorous stirring under nitrogen for 15 min. A toluene

solution of the oleic acid-capped UCNPs (50 mg in 2 mL) was quickly injected into the hot solution and allowed to evaporate for 15 min. Then the system was heated to 240 °C for 2 h at reflux under nitrogen. The reaction mixture was cooled to room temperature. A dilute hydrochloric aqueous solution was added in excess to the reaction mixture, which was then stirred for 30 min. A white powder was obtained via centrifugation. The powder was washed three times with pure water to remove excess PAA and could be well dispersed in water, an aqueous buffer and alcohol.

2.4. Attachment of amino aptamers to the upconversion nanoparticles

The preparation of the aptamers-conjugated UCNPs was adapted from a previously reported method [34]. For the $NaYF_4$: Yb, Ho UCNPs, for example, 10 mg of PAA-modified UCNPs was first dispersed in 5 mL of a 10 mM PBS buffer solution (pH 7.4), and then 0.8 mL of EDC (2 mg mL^{-1}) and 0.4 mL of NHS (2 mg mL^{-1}) were added to the solution. The reaction was continued for 2 h at 37 °C with gentle shaking, and UCNPs were separated by centrifugation and washed with ultrapure water for three times. Next, the activated PAA-UCNPs were dispersed in 5 mL of a PBS buffer solution. Then, 50 μL of 100 μM amino-modified aptamers were added. The mixture was then incubated at 37 °C with oscillation for another 2 h. After removing the supernatant, the aptamers-modified UCNPs were washed twice with a PBS buffer by centrifugation and redispersion and then finally redispersed in fresh binding buffer (10 mM Tris–HCl, pH 7.4, 100 mM KCl and 1 mM $MgCl_2$). Apt_1 was conjugated to $NaYF_4$: Yb, Ho UCNPs, and Apt_2 was conjugated to Mn^{2+}-doped $NaYF_4$: Yb, Er UCNPs. In the optimized procedure, the concentrations of the aptamers-modified $NaYF_4$: Yb, Ho UCNPs and Mn^{2+}-doped $NaYF_4$: Yb, Er UCNPs were approximately 2 mg mL^{-1} and 1.6 mg mL^{-1}, respectively.

2.5. Synthesis of gold nanoballs/gold nanorods and thiolated oligonucleotides conjugation

All glassware was cleaned in aqua regia (HCl/HNO_3, 3:1), rinsed with triply distilled H_2O and then oven-dried prior to use. The 15 nm gold nanoballs were synthesized using a common method, reducing developed gold ions with sodium citrate [42]. In this procedure, 95.8 mL of triply distilled H_2O and 4.2 mL of 1% $HAuCl_4$ were boiled with vigorous stirring for 10 min, and 10 mL of 1% trisodium citrate was added rapidly under stirring. The solution turned blue within 25 s; the final color change to red–violet occurred 1 min later. The solution was boiled for an additional 10 min. Then, the heating source was removed, and the colloid was stirred for another 15 min. The solution was then allowed to cool to room temperature. The water-soluble gold nanorods were synthesized via seed-mediated growth routes according to the literature methods [35,43]. First, the seed solution, which was a mixture of equal volumes of 0.5 mM $HAuCl_4$ and 0.2 M CTAB, was prepared under vigorous magnetic stirring. Then ice-cold 0.01 M $NaBH_4$ (0.6 mL) was added, and the resulting seed solution turned brownish yellow. The seed solution was vigorously stirred for 2 min and then kept at 25 °C. Second, the growth solution was synthesized as follows: CTAB (0.2 M, 5.0 mL) was added to 5.0 mL of a 0.5 mM $HAuCl_4$ solution at 25 °C. To this solution, 0.1 mL of 4 mM $AgNO_3$ was added, and after gentle mixing of the solution, 70 μL of 0.0788 M ascorbic acid was added. Ascorbic acid acted as a mild reducing agent and rapidly changed the growth solution from dark yellow to colorless. Finally, 12 μL of the seed solution was added to the growth solution at 27–30 °C. The color of the solution gradually changed to dark cyan over approximately 20 min. The solution was then centrifuged to remove the excessive CTAB.

The procedure for conjugating the gold nanoparticles to oligonucleotides was adapted from the previously reported protocol [44,45]. This protocol was based on the Au–S interaction between the gold lattice and thiolated oligonucleotides. Briefly, 10 μL of 100 μM $cDNA_1$ was added to 1 mL of the gold nanoballs solution, and similarly, 10 μL of 100 μM $cDNA_2$ was added to 1 mL of the gold nanorods solution. After reacting for 16 h, the AuNPs–oligonucleotides complexes were "aged" with salts (0.1 M NaCl, 10 mM phosphate, pH 7.0) for 40 h. The solution was then centrifuged at 12,000 rpm for 15 min. The supernatant was removed, and the solid at the bottom of the tube was dispersed in the binding buffer (10 mM Tris–HCl, pH 7.4, 100 mM KCl and 1 mM $MgCl_2$) for subsequent experiments.

2.6. Procedure for the simultaneous detection of Pb^{2+} and Hg^{2+}

A typical FRET analysis was performed according to the following steps. First, 200 μL of Apt_1-functionalized $NaYF_4$: Yb, Ho UCNPs and Apt_2-functionalized Mn^{2+}-doped $NaYF_4$: Yb, Er UCNPs were mixed and then 200 μL of $cDNA_1$-functionalized gold nanoballs and $cDNA_2$-functionalized gold nanorods were added. The mixture was incubated at 37 °C for 2 h. Specific amounts of Pb^{2+} and Hg^{2+} standard solutions were subsequently added to the mixture, which was further incubated at 37 °C for 40 min. The upconversion fluorescence spectra of the final mixture were then measured using an F-7000 fluorescence spectrometer with an external 980 nm laser as the excitation source in place of the xenon lamp in the spectrometer.

2.7. Real sample preparation and measurements

25 g shrimp or fish was aseptically dipped in 225 mL PBS pH 7.4 and homogenized for 5 min. The product was left to stand for 30 min to precipitate macroaggregates and seston. The supernatant was subsequently filtered through a 0.45 μm filtration membrane. To avoid sample clotting, the plasma samples from the Fourth Affiliated Hospital of Soochow University were pretreated by first removing fibrinogen via precipitation according to the reported literature method [46]. In short, 1.25 mL ammonium sulfate (2 M) and 1 mL NaCl (0.1 M) were mixed with 0.25 mL of plasma. Several minutes later, the mixture was centrifuged, and the supernatant was retained for further experiments. The spiked samples were then analyzed using the method described previously.

3. Results and discussion

3.1. Principles of the dual FRET assay for the simultaneous detection of $Pb^{2\pm}$ and $Hg^{2\pm}$

The assay protocol for simultaneously detecting Pb^{2+} and Hg^{2+} using the dual FRET system based on two color UCNPs and controlled AuNPs is depicted schematically in Fig. 1. First, the amino-modified aptamers were covalently attached to the carboxyl-functionalized UCNPs, and the thiol-modified complementary DNA of the aptamers was conjugated to the controlled AuNPs through strong Au–S bonds. Second, the dual FRET system was established between two donor–acceptor pairs: Apt_1-functionalized $NaYF_4$: Yb, Ho UCNPs hybridized with $cDNA_1$-functionalized gold nanoballs and Apt_2-functionalized Mn^{2+}-doped $NaYF_4$: Yb, Er UCNPs hybridized with $cDNA_2$-functionalized gold nanorods. (The DNA sequences are shown in Table 1.) Thus, the energy donors and acceptors were placed in close proximity, and the green and red upconverison fluorescence could be quenched by the gold nanoballs and nanorods due to their highly overlapped spectrums. More importantly, the two donor–acceptor pairs were

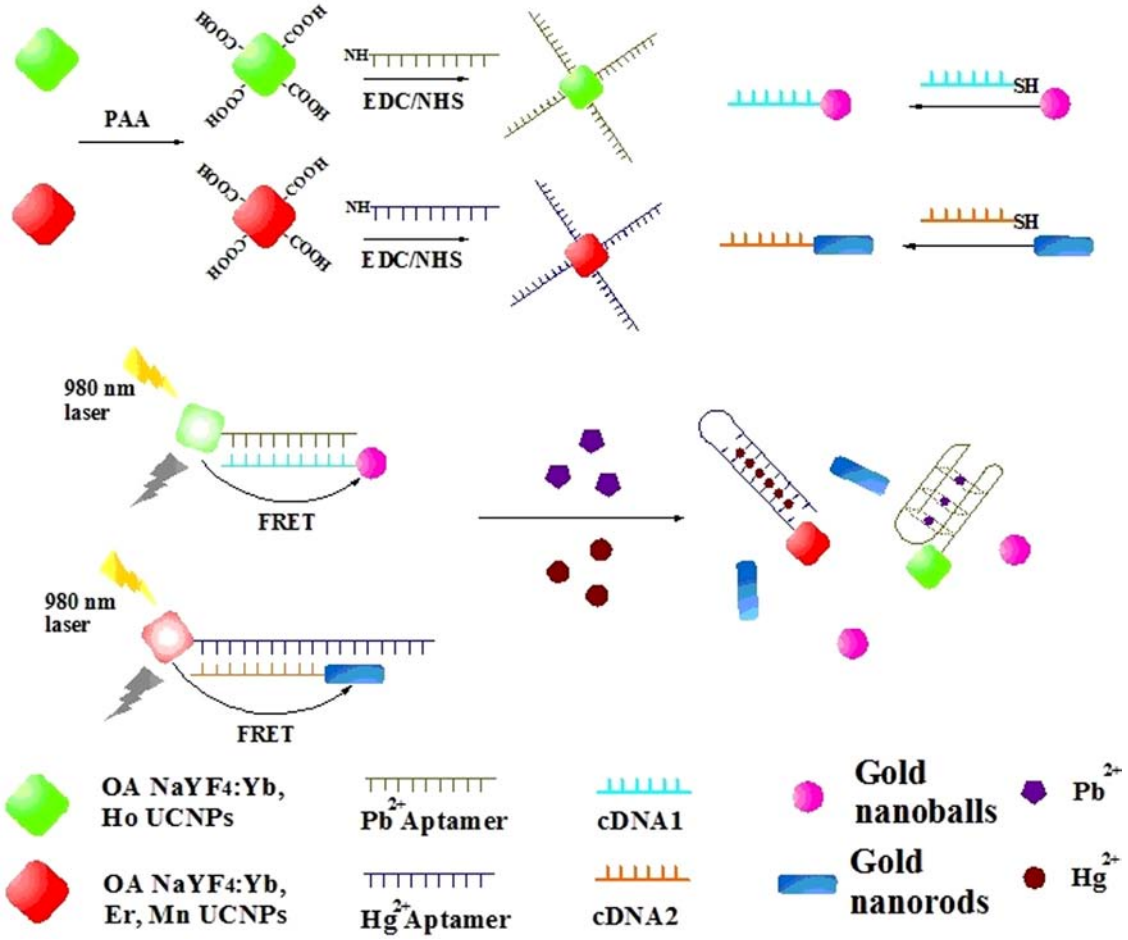

Fig. 1. Schematic illustration of dual FRET between the upconversion nanoparticles and controlled gold nanoparticles for the simultaneous detection of Pb^{2+} and Hg^{2+}.

independent and did not interfere with each other because each complementary DNA was specially designed to match the corresponding aptamer. Third, in the presence of Pb^{2+} and Hg^{2+}, the aptamers preferred to bind to their corresponding analytes, which led to changes in the aptamer conformations and induced the formation of intermolecular G-quadruplex [17–20,47–49] and hairpin-like structures [50–53]. Specifically, the binding of Apt_1 to Pb^{2+} resulted in the formation of G-quadruplexes and induced the dehybridization of the $cDNA_1$-functionalized gold nanoballs. This effect became sufficiently large to prevent fluorescence quenching, and thus, the green fluorescence was recovered. For Hg^{2+}, thymine (T) has been demonstrated to be one of the most specific ligands for Hg^{2+} and can form a T–Hg^{2+}–T complex with strong affinity and high selectivity. Thus, the formation of this complex displaced the $cDNA_2$-functionalized gold nanorods, which were then released from the Mn^{2+}-doped $NaYF_4$: Yb, Er UCNPs. As a result, the red fluorescence signal increased. Finally, the restoration of the upconverison fluorescence intensity was a function of the Pb^{2+} and Hg^{2+} concentrations.

3.2. Characterization of upconversion nanoparticles and gold nanoparticles

In this work, UCNPs were synthesized by a hydrothermal route in the presence of oleic acid. Fig. 2a–d shows representative TEM images of the oleic acid-capped UCNPs and PAA-modified samples. The monodisperse 20–30 nm nanocubes of the as-prepared samples suggested that the long-chain oleic acid ligands on the crystal surface prevented aggregation. However, the UCNPs must be dispersed in water for bio-applications, and thus, their surfaces were modified with hydrophilic groups. To convert the hydrophobic oleic acid-capped UCNPs into their carboxylic acid-functionalized derivatives, PAA was used as a multidentate ligand to displace the original hydrophobic ligand on the UCNPs surface and allow the UCNPs to be dispersed in water. After the ligand exchange, the PAA-modified samples still consisted primarily of single nanocubes; however, the formation of nanoarrays was prevented by the carboxylic acid interactions. These observations indicated that the oxidation only affected the UCNPs array formation but not their size or shape. The fluorescence intensity of the modified samples remained nearly constant. The gold nanoballs were approximately 15 nm, and the gold nanorods had a width of 9–10 nm and length of 35 ± 5 nm (Fig. 2e and f). Their stability and water solubility were good.

The capping ligands on the surface of UCNPs were identified by FT-IR spectroscopy (Fig. S1). The prominent transmission bands at 2924 and 2854 cm^{-1} in the oleic acid-capped UCNPs were respectively corresponded to the asymmetric and symmetric stretching vibrations of the methylene ($-CH_2-$) in the long alkyl chain, and two strong bands centered at 1564 and 1463 cm^{-1} which were associated with the asymmetric and symmetric stretching vibrations of the carboxylate anions on the surface of the UCNPs before the ligand exchange, were also observed in the spectrum. A peak at 3007 cm^{-1} attributed to the =C–H stretching vibration was clearly observed in the spectrum of the as-prepared sample (Fig. S1a). However, for the PAA-modified sample, this feature apparently disappeared after ligand exchange (Fig. S1b and c), which suggested the cleavage of the –HC=CH– group. Additionally,

the shoulder peak at ~2929 cm^{-1} associated with the asymmetrical stretching of the $-CH_2-$ groups was reduced. Meanwhile, the strong bands at ~1725 cm^{-1} indicated an increase in the quantity of carboxyl groups on the particle surface. Therefore, it was concluded that PAA replaced the oleate anions on the UCNPs surface.

The powder X-ray diffraction (XRD) pattern of the synthesized material had well-defined peaks, indicating it was crystalline. The reaction time and temperature influenced the UCNP phase transition. Fig. S2 displays the XRD patterns of the UCNPs synthesized at 190 °C for 12 h. It was observed that $NaYF_4$: Yb, Ho UCNPs can be ascribed to hexagonal (JCPDS file number 16-0334) phases of $NaYF_4$. The pure cubic $NaYF_4$ (JCPDS file number 77-0242) was obtained when the presence of Mn^{2+} ions reached 30 mol% in the $NaYF_4$: Yb, Er UCNPs and no obvious extra diffraction peaks were detected due to the substitution of Y^{3+} ions with smaller Mn^{2+} ions in the host lattice.

It is well known that gold nanoparticles exhibit good absorption properties in the visible region. The gold nanoballs suspension used in this work displayed a strong absorption band at approximately 525 nm (Fig. 3a). In the Yb^{3+} and Ho^{3+} co-doped systems, a single green emission at 542 nm was observed in the

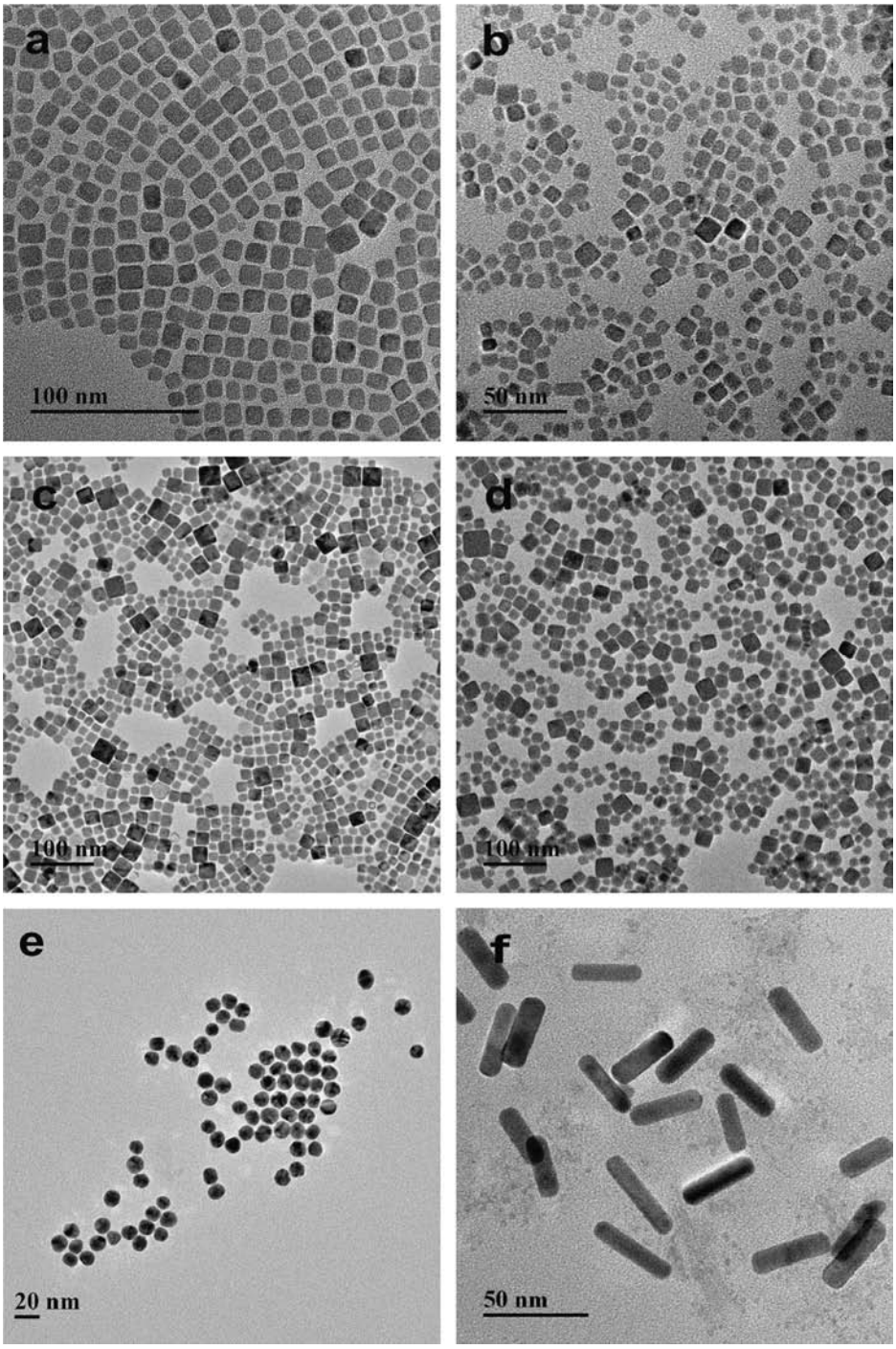

Fig. 2. Morphology and dispersibility study. High resolution TEM images of oleic acid-capped $NaYF_4$: Yb, Ho UCNPs (a) and oleic acid-capped Mn^{2+}-doped $NaYF_4$: Yb, Er UCNPs (c) dispersed in cyclohexane, after ligand-exchange, PAA modified $NaYF_4$: Yb, Ho UCNPs (b) and PAA-modified Mn^{2+}-doped $NaYF_4$: Yb, Er UCNPs (d) dispersed in aqueous solutions, gold nanoballs (e) and gold nanorods (f).

fluorescence spectrum (Fig. 3b). Thus, FRET possibly resulted between the $NaYF_4$: Yb, Ho UCNPs (donor) and the gold nanoballs (acceptor) possibly. On the other hand, gold nanorods typically exhibited two surface plasma resonance (SPR) modes, a transverse mode and a longitudinal mode, resulting in two resonance absorption bands at 515 and 692 nm (Fig. 3c), respectively. In our work, we employed the longitudinal SPR band located at approximately 692 nm as the energy acceptor, which nearly overlapped the upconversion fluorescence emission of the energy donor Mn^{2+}-doped $NaYF_4$: Yb, Er UCNPs at 660 nm (Fig. 3d). More importantly, the green and red emission peaks had large Stokes shifts and could be clearly distinguished from each other. The groups of tunable UCNPs and controlled AuNPs were essential to enable simultaneous detection.

3.3. Characterization of the nanoparticles conjugated to oligonucleotides

The aptamers were conjugated to the upconversion nanoparticle surfaces through the amino-carboxyl reaction illustrated in Fig. 1. The preparation process included ligand exchange and surface activation as previously mentioned. To verify that the UCNPs were functionalized with aptamers, UV–vis absorption spectroscopy and zeta potential measurements were utilized to monitor the reaction products, and the results are shown in Fig. 4 and S3. No absorption peak was detected for the carboxyl-functionalized UCNPs (both $NaYF_4$: Yb, Ho UCNPs and Mn^{2+}-doped $NaYF_4$: Yb, Er UCNPs). After conjugation to the amino-modified aptamers, a new absorption peak at approximately 260 nm was observed due to the ultraviolet absorption spectrum of DNA (Fig. 4a and b). Zeta potential experiments indicated that the PAA-modified $NaYF_4$: Yb, Ho UCNPs were negatively charged, and the zeta potential varied from −31.3 mV to −23.2 mV after conjugation to the aptamers (Fig. S3a). Similarly, the Mn^{2+}-doped $NaYF_4$: Yb, Er UCNPs were conjugated to amino aptamers; the zeta potential was positively shifted to −22.7 mV (Fig. S3b). These results also demonstrated that the nanoparticles were successfully functionalized with amino aptamers.

Similarly, a new DNA absorption peak appeared at approximately 260 nm after incubating the gold nanoparticles with thiolated oligonucleotides, which were conjugated due to Au–S interactions (Fig. 4c and d). The zeta potential of the bare gold nanoballs was −42.3 mV; after incubation, the zeta potential of the DNA–gold nanoballs was approximately −33.4 mV (Fig. S3c). The zeta potential of the bare gold nanorods was positively

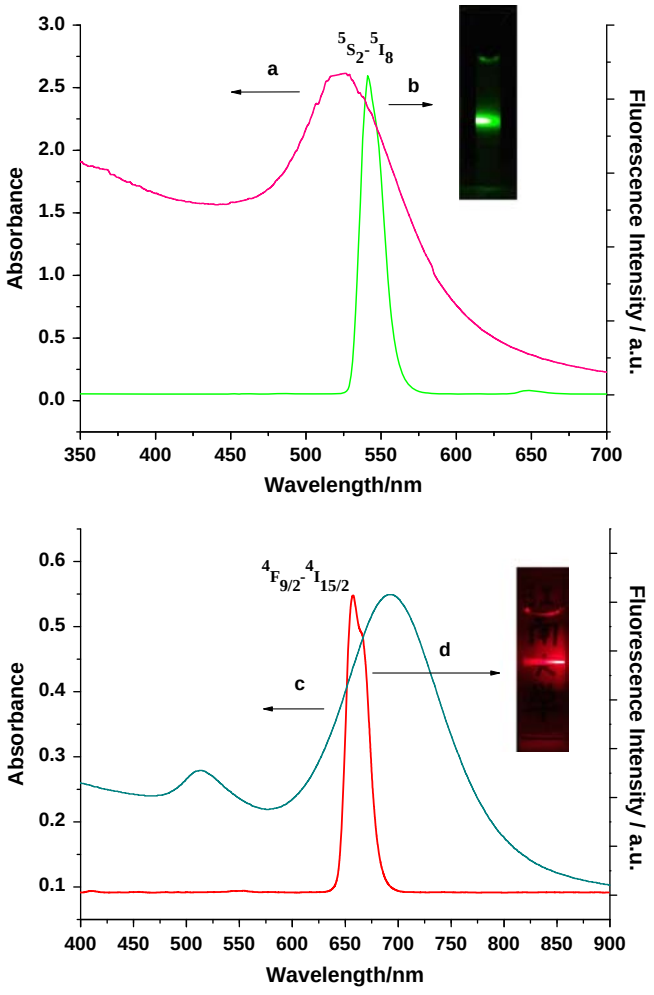

Fig. 3. UV–vis absorption spectra of gold nanoballs (a), and gold nanorods (c); upconversion fluorescence emission spectra of $NaYF_4$: Yb, Ho UCNPs (b), and Mn^{2+}-doped $NaYF_4$: Yb, Er UCNPs (d). Photograph of naked-eye visible green and red upconversion fluorescence excited by a 980 nm laser in a transparent aqueous colloid solution.

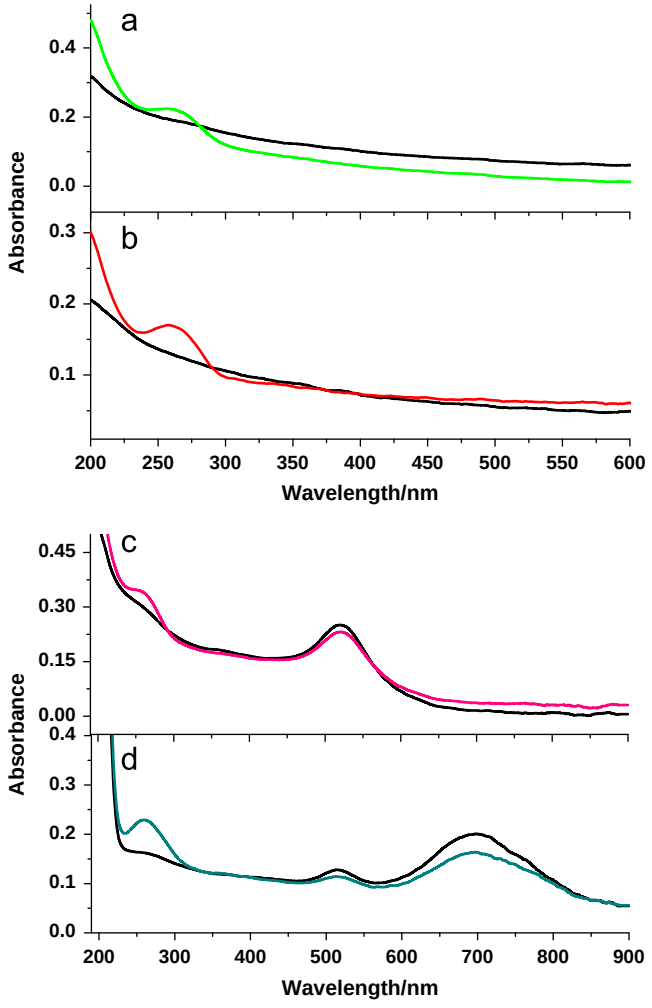

Fig. 4. UV–vis absorption spectra of bare $NaYF_4$: Yb, Ho UCNPs (black line in a) and aptamers-functionalized $NaYF_4$: Yb, Ho UCNPs (green line in a), bare Mn^{2+} ions doped $NaYF_4$: Yb, Er UCNPs (black line in b) and aptamers-functionalized Mn^{2+} ions doped $NaYF_4$: Yb, Er UCNPs (red line in b); bare gold nanoballs (black line in c) and $cDNA_1$-functionalized gold nanoballs (pink line in c), bare gold nanorods (black line in d) and $cDNA_2$-functionalized gold nanorods (dark cyan line in d). (For interpretation of the references to color in this figure legend, the reader is referred to the web version of this article.)

charged because of CTAB, which acted as a cationic surface active agent, on the nanorod surfaces. However, the zeta potential was negatively shifted to −8.61 mV after conjugation to thiolated oligonucleotides (Fig. S3d). Therefore, the results demonstrated that both DNA–AuNPs complexes were successfully formed.

3.4. Optimization of the assay conditions

In this system, several factors that might affect the detection sensitivity, such as the concentrations of the energy donors and acceptors, incubation time, pH and incubation temperature were studied. Specifically, various concentrations of the aptamers-modified UCNPs were hybridized with the cDNA-modified AuNPs to fabricate the FRET system, and then the fluorescence was restored after adding Pb^{2+} and Hg^{2+}. Fig. 5 shows the effect of different concentrations of UCNPs on the analyte response. When the UCNPs concentration was too low, the relative excess of aptamers could not attach to the UCNPs surface. As a result, many free aptamers hybridized with the complementary DNA, and they could not fabricate FRET between the UCNPs and AuNPs. When UCNPs were in relative excess, the free UCNPs also could not fabricate the FRET without binding to aptamers. To increase the sensitivity of the FRET aptasensor, the concentrations of 2 mg mL^{-1} and 1.6 mg mL^{-1} were chosen for the $NaYF_4$: Yb, Ho UCNPs and Mn^{2+}-doped $NaYF_4$: Yb, Er UCNPs, respectively. Furthermore, the incubation time and buffer solution required for aptamer recognition of the analytes was based on the literature values [17,19,48]. Thus, for the Pb^{2+} and Hg^{2+} aptamers, an incubation time of 40 min and binding buffer (10 mM Tris–HCl, pH 7.4, 100 mM KCl and 1 mM $MgCl_2$) were adopted in this assay. In addition, incubation temperature of aptamers binding with analytes was selected. The results showed that there was no difference whether the temperature is 37 °C or 25 °C (Fig. S4.). Therefore, 37 °C was chosen for the experiment in order to consistent with the hybrid temperature.

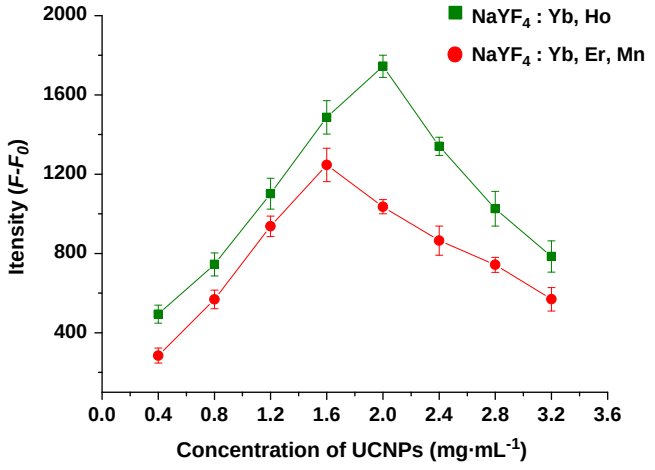

Fig. 5. The restoration of the fluorescence intensity after incubation with the analytes as a function of the concentration of the donor probes (UCNPs) in the FRET system. Both Pb^{2+} and Hg^{2+} were 10 nM.

3.5. Control experiments

To confirm the dual FRET and recognition reaction between the UCNPs and controlled AuNPs, a series of control experiments were performed. As shown in Fig. 6A, a mixture of $NaYF_4$: Yb, Ho UCNPs and Mn^{2+}-doped $NaYF_4$: Yb, Er UCNPs exhibited two strong fluorescence signals at 542 nm and 660 nm when excited with a 980 nm laser. When bare gold nanoballs and nanorods were added, no obvious changes in the fluorescence intensities were observed, indicating that the bare UCNPs and bare AuNPs did not interact. Although the UCNPs fluorescence intensity decreased slightly, the decrease was negligible compared to that observed when FRET occurred. For the aptamer–UCNPs and oligonucleotide–AuNPs mixture, the two UCNPs fluorescence emission peaks decreased dramatically through the hybridization of the UCNPs and AuNPs.

Further investigations (Fig. 6B) showed that when only the $cDNA_1$-gold nanoballs were present, the fluorescence of the $NaYF_4$: Yb, Ho UCNPs was quenched effectively, and the peak at 660 nm was not affected. On the contrary, when only the $cDNA_2$-gold nanorods were added, the fluorescence of the Mn^{2+}-doped

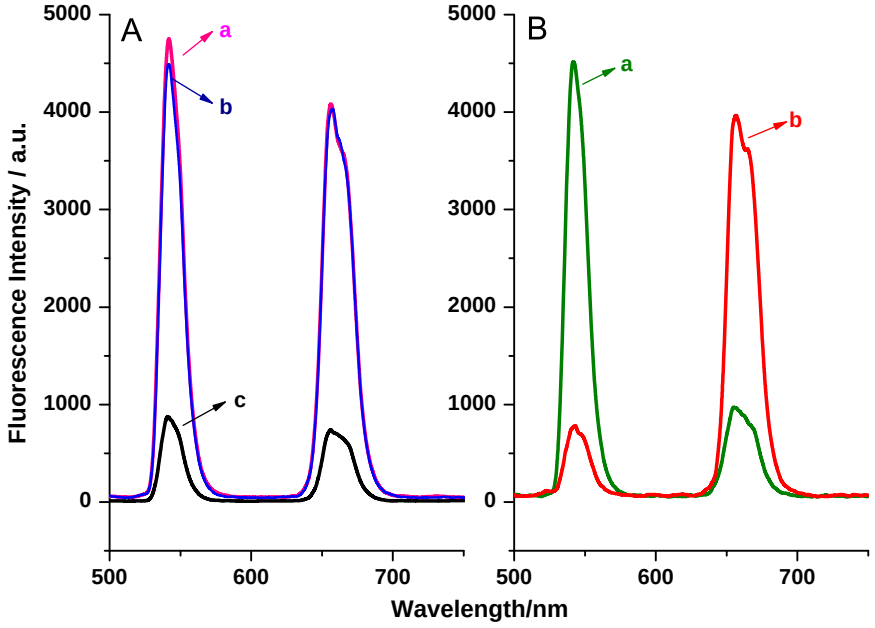

Fig. 6. Fluorescence emission spectra A: $NaYF_4$: Yb, Ho and Mn^{2+}-ions doped $NaYF_4$: Yb, Er UCNPs UCNPs (a), (a)+gold nanoballs and gold nanorods (b), aptamers-functionalized UCNPs ybridized with cDNA-functionalized AuNPs (c). Fluorescence emission spectra B: two types of aptamers functionalized UCNPs hybridized with $cDNA_2$-functionalized gold nanorods (a) and $cDNA_1$-functionalized gold nanoballs (b).

$NaYF_4$: Yb, Er UCNPs was quenched, and the fluorescence at 542 nm was still observed. It was verified that the $NaYF_4$: Yb, Ho UCNPs and gold nanoballs and the Mn^{2+}-doped $NaYF_4$: Yb, Er UCNPs and gold nanorods constituted two donor–acceptor pairs that were independent and did not interfere with each other. In summary, these control experiments confirmed that the controlled AuNPs and UCNPs played important roles during the construction of the dual FRET system and fabrication of the simultaneous detection abilities.

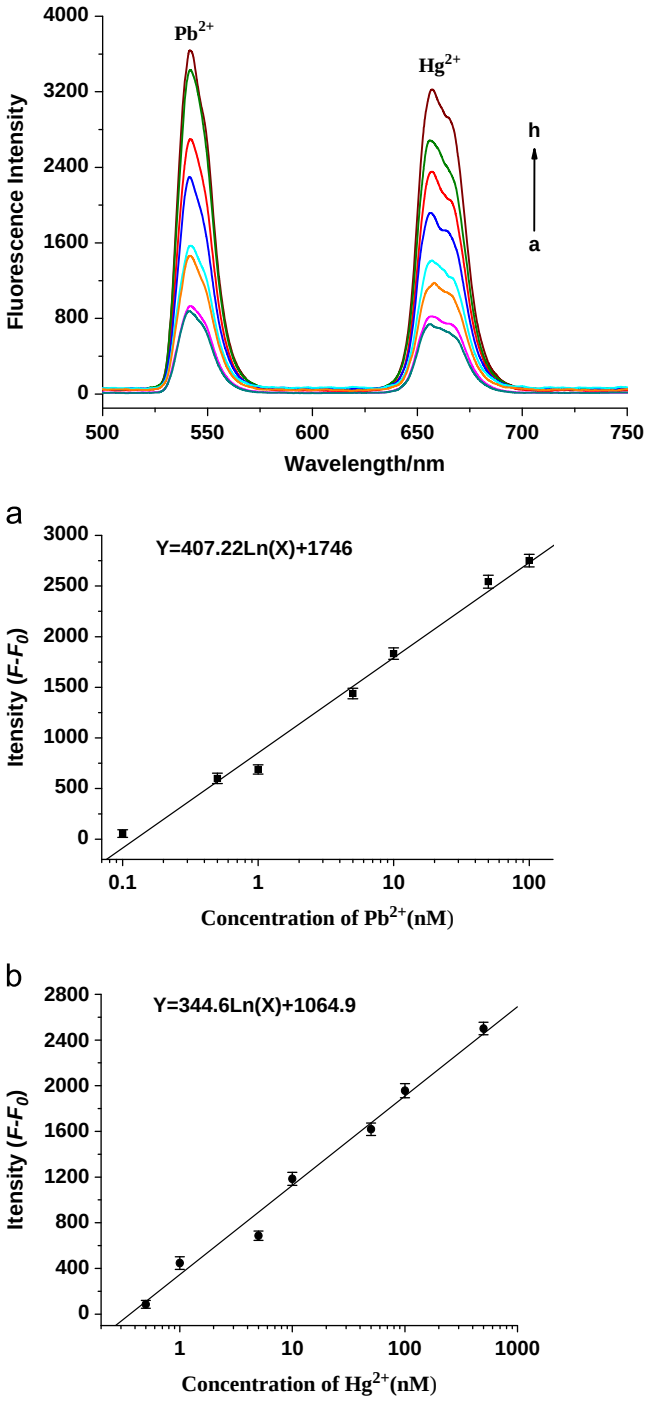

Fig. 7. Typical recording output for the simultaneous detection of different concentrations of Pb^{2+} or Hg^{2+} using the developed method (a-h: 0.1, 0.5, 1, 5, 10, 50, 100 and 500 nM). Standard curve of the fluorescence intensity (F–F_0) versus the Pb^{2+} concentration (a) and Hg^{2+} (b) concentrations were measured using the developed method.

3.6. Quantitative detection of Pb^{2+} and Hg^{2+}

The upconversion fluorescences at 542 nm and 660 nm were chosen to monitor Pb^{2+} and Hg^{2+}, respectively. The detection of Pb^{2+} and Hg^{2+} under optimal conditions was performed, as the Pb^{2+} and Hg^{2+} concentrations increased, the upconversion fluorescence signals gradually increased (Fig. 7). The metal ion concentrations were proportional to the increase in the fluorescence intensity (ΔF), where ΔF is the difference in the upconversion fluorescence intensity excited by a 980 nm laser in the absence and presence of Pb^{2+} or Hg^{2+}. The calibration curve of the relationship between the relative intensity of the upconversion fluorescence and Pb^{2+} concentration ranged from 0.1 nM to 100 nM (Y=407.22Ln(x)+1746, R=0.9950, Fig. 7a) and from 0.5 nM to 500 nM for Hg^{2+} (Y=344.6Ln(x)+1064.9, R=0.9930, Fig. 7b). Statistical analysis revealed that the detection limits of Pb^{2+} and Hg^{2+}, which were estimated to be 3σ, were 50 pM and 150 pM, respectively. The precision, expressed as the relative standard deviation (RSD) in the Pb^{2+} detection, was equal to 5.84% (10 nM, n=7). The RSD in the Hg^{2+} detection was equal to 7.12% (10 nM, n=7), indicating that the developed method exhibited good reproducibility.

3.7. Specificity evaluation for the assay

To test the selectivity of the assay for Pb^{2+} and Hg^{2+}, the effects of other metal ions (K^+, Na^+, Ca^{2+}, Cd^{2+}, Cu^{2+}, Co^{2+}, Mg^{2+}, Ba^{2+}, Fe^{3+}, Mn^{2+} and Al^{3+}) on the FRET were evaluated. Each type of metal ion was added to the prepared detection system individually, and after incubation, the efficiency of the fluorescence restoration was recorded. The experimental results shown in Fig. 8 indicate that only Pb^{2+} and Hg^{2+} induced a dramatic fluorescence enhancement at their corresponding peaks. None of the other metal ions generated significant fluorescence signals, even at concentrations as high as 10 mM of K^+, Na^+, Ca^{2+}, and Mg^{2+}, 1 mM of Fe^{3+}, Al^{3+} Cu^{2+}, Ba^{2+}, and Mn^{2+}, and 10 μM of Cd^{2+}, and Co^{2+}, indicating that only Pb^{2+} and Hg^{2+} could induce changes in the structural conformations of the aptamers. In addition, chlorate solution such as NaCl, KCl, $MgCl_2$, $FeCl_3$, $BaCl_2$ and others were tested as interferences. The results showed that they could not react with $Pb(NO_3)_3$ and $Hg(NO_3)_3$, and could not form precipitate in salt solution. Therefore, some chloride could not interfere with our proposed method. The results clearly demonstrated this dual FRET assay has high anti-interference capabilities and excellent specificity.

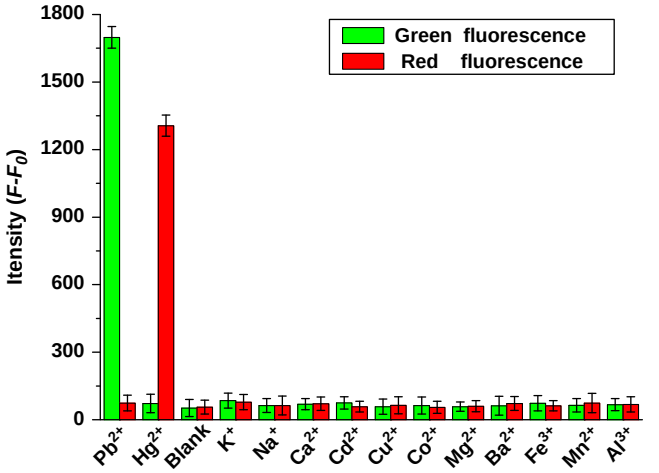

Fig. 8. The response signal change in the upconversion fluorescence with various metal ions as interferents.

Table 2
Comparison between the developed method and AAS method for application in sea food and human serum, and recovery results for the spiked Pb^{2+} and Hg^{2+} in real samples using the developed method.

Sample	Analytes	Background content (nM)	Added concentration (nM)	AAS (nM)	Detected by the proposed method (nM)	Recovery ratio (%)
Fish	Pb^{2+}	3.24	5	8.56	8.18	98.8
	Hg^{2}	4.67	5	9.18	9.24	91.4
	Pb^{2+}	3.18	10	13.57	13.57	103.9
	Hg^{2}	2.98	10	12.77	12.36	93.8
	Pb^{2+}	12.24	10	22.33	21.87	96.3
Shrimp	Hg^{2}	7.81	10	17.14	18.04	102.3
	Pb^{2+}	5.15	50	54.26	55.96	101.62
	Hg^{2}	4.21	50	54.67	53.31	98.2
	Pb^{2+}	9.24	5	15.02	14.77	110.6
Human serum	Hg^{2}	2.36	5	7.15	7.42	101.2
	Pb^{2+}	10.24	50	61.03	59.34	98.2
	Hg^{2}	ND	50	49.27	50.97	101.94

ND = not detect.
Recovery ratio % = (Detected by proposed method − Background content)/Added concentration × 100.

3.8. Analytical applications

The feasibility of applying the multiplexed FRET-based assay to measure Pb^{2+} and Hg^{2+} levels in naturally contaminated samples was validated using 6 specimens including sea food and human serum. These specimens were measured using our new approach and an available atomic absorption spectrometry method. The results in Table 2 show that there was no significant difference between the two methods and that they were highly correlated ($R^2 = 0.9973$, $P < 0.0001$). The Pb^{2+} recovery values were between 96.3% and 110.6%, and the Hg^{2+} recovery values were between 91.4% and 102.3%, indicating that the developed assay is highly accurate. These analyses demonstrated that the proposed method can be used to detect Pb^{2+} and Hg^{2+} in foodstuff applications and human serum samples.

4. Conclusions

In summary, this work introduced a novel dual FRET assay that uses UCNPs–aptamers–AuNPs ensembles to detect Pb^{2+} and Hg^{2+} simultaneously. This approach exhibited excellent sensitivity and selectivity because of the superior optical features of UCNPs and the high affinity and specificity of the aptamers, which could form G-quadruplexes and T–Hg^{2+}–T complexes. Furthermore, two upconversion fluorescence peaks, which were excited by a uniform 980 nm laser, acted as donors, and gold nanoballs and nanorods quenched the corresponding fluorescence. Based on these two donor–acceptor pairs, this dual FRET system was built to detect Pb^{2+} and Hg^{2+} simultaneously. This method demonstrated the potential for use in practical applications, such as detecting metal ions in the environment and foodstuff or clinical diagnosis, especially when Pb^{2+} and Hg^{2+} coexist. The platform of this dual FRET system is a promising general optical sensing strategy for the detection of other contaminants in food samples.

Acknowledgments

This work was partly supported by NSFC (21375049), the S&T Supporting Project of Jiangsu Province (BE2011621), National Science and Technology Support Program of China (2012BAK08B01), and Research Fund for the Doctoral Program of Higher Education (20110093110002), NCET-11-0663, JUSRP11436, and JUSRP51309A.

Appendix A. Supporting information

Supplementary data associated with this article can be found in the online version at http://dx.doi.org/10.1016/j.talanta.2014.04.056.

References

[1] L.B. Xia, X. Li, Y.L. Wu, B. Hu, R. Chen, Spectrochim. Acta B 63 (2008) 1290–1296.
[2] W.H. Hsu, S.J. Jiang, A.C. Sahayam, Talanta 117 (2013) 268–272.
[3] R. Gao, Z. Hu, X.J. Chang, Q. He, L.J. Zhang, Z.F. Tu, J.P. Shi, J. Hazard. Mater. 172 (2009) 324–329.
[4] P.C. Li, S.J. Jiang, Anal. Chim. Acta 495 (2003) 143–150.
[5] L.R. Bravo-Sanchez, B.S. de la Riva, J.M. Costa-Fernandez, R. Pereiro, A. Sanz-Medel, Talanta 55 (2001) 1071–1078.
[6] P. Bermejo-Barrera, M.C. Barciela-Alonso, J. Moreda-Pineiro, C. Gonzalez-Sixto, A. Bermejo-Barrera, Spectrochim. Acta B 51 (1996) 1235–1244.
[7] M. Ceulemans, F.C. Adams, J. Anal. At. Spectrom. 11 (1996) 201–206.
[8] G.Y. Yang, C.M. Zhang, Q.F. Hu, J.Y. Yin, J. Chromatogr. Sci. 41 (2003) 195–199.
[9] W. Yantasee, Y.H. Lin, T.S. Zemanian, G.E. Fryxell, Analyst 128 (2003) 467–472.
[10] P.H. Zhang, S.Y. Dong, G.Z. Gu, T.L. Huang, Bull. Korean Chem. Soc. 31 (2010) 2949–2954.
[11] Y. Wei, C. Gao, F.L. Meng, H.H. Li, L. Wang, J.H. Liu, X.J. Huang, J. Phys. Chem. C 116 (2012) 1034–1041.
[12] M. Zhang, L. Ge, S.H. Ge, M. Yan, J.H. Yu, J.D. Huang, S. Liu, Biosens. Bioelectron. 41 (2013) 544–550.
[13] M.A. Rahman, M.S. Won, Y.B. Shim, Anal. Chem. 75 (2003) 1123–1129.
[14] Z.Z. Lin, X.H. Li, H.B. Kraatz, Anal. Chem. 83 (2011) 6896–6901.
[15] C.W. Lien, Y.T. Tseng, C.C. Huang, H.T. Chang, Anal. Chem. 86 (2014) 2065–2072.
[16] Y. Zhou, Y.S. Li, X.Y. Meng, Y.Y. Zhang, L. Yang, J.H. Zhang, X.R. Wang, S.Y. Lu, H.L. Ren, Z.S. Liu, Sensor Actuat. B-Chem 183 (2013) 303–309.
[17] Y.W. Lin, C.W. Liu, H.T. Chang, Talanta 84 (2011) 324–329.
[18] S.J. Xiao, P.P. Hu, G.F. Xiao, Y. Wang, Y. Liu, C.Z. Huang, J. Phys. Chem. B 116 (2012) 9565–9569.
[19] C.W. Liu, C.C. Huang, H.T. Chang, Anal. Chem. 81 (2009) 2383–2387.
[20] C.H. Chung, J.H. Kim, J. Jung, B.H. Chung, Biosens. Bioelectron. 41 (2013) 827–832.
[21] F. Auzel, Chem. Rev. 104 (2004) 139–173.
[22] K. Kuningas, T. Rantanen, T. Ukonaho, T. Lovgren, T. Soukka, Anal. Chem. 77 (2005) 7348–7355.
[23] L.Y. Wang, R.X. Yan, Z.Y. Huo, L. Wang, J.H. Zeng, Y.D. Li, Angew. Chem. Int. Ed. 44 (2005) 6054–6057.
[24] L. Wang, Y. Li, Chem. Commun. 24 (2006) 2557–2559.
[25] Y.X. Ma, L.Y. Wang, Talanta 120 (2014) 100–105.
[26] Z.J. Wang, L.N. Wu, B.Z. Shen, Z.H. Jiang, Talanta 114 (2013) 124–130.
[27] X.Y. Huang, J.J. Wang, H. Liu, T. Lan, J.C. Ren, Talanta 106 (2013) 79–84.
[28] H.Q. Chen, J.C. Ren, Talanta 99 (2012) 404–408.
[29] M. Wang, C.C. Mi, Y.X. Zhang, J.L. Liu, L. Feng, C.B. Mao, S.K. Xu, J. Phys. Chem. C 113 (2009) 19021–19027.
[30] Q.B. Zhang, X. Wang, Y.M. Zhu, J. Mater. Chem. 21 (2011) 12132–12138.
[31] Z.Q. Li, Y. Zhang, Angew. Chem. Int. Ed. 4 (2006) 7732–7735.
[32] S.J. Wu, N. Duan, C.Q. Zhu, X.Y. Ma, M. Wang, Z.P. Wang, Biosens. Bioelectron. 30 (2011) 35–42.
[33] S.J. Wu, N. Duan, Z.P. Wang, H.X. Wang, Analyst 136 (2011) 2306–2314.
[34] S.J. Wu, N. Duan, X.Y. Ma, Y. Xia, H.X. Wang, Z.P. Wang, Q. Zhang, Anal. Chem. 84 (2012) 6263–6270.

[35] B. Nikoobakht, M.A. El-Sayed, Chem. Mater. 15 (2003) 1957–1962.
[36] J.H. Peng, Y.H. Wang, J.L. Wang, X. Zhou, Z.H. Liu, Biosens. Bioelectron. 28 (2011) 414–420.
[37] H.Q. Chen, F. Yuan, S.Z. Wang, J. Xu, Y.Y. Zhang, L. Wang, Biosens. Bioelectron. 48 (2013) 19–25.
[38] H.Q. Chen, F. Yuan, S.Z. Wang, J. Xu, Y.Y. Zhang, L. Wang, Analyst 138 (2013) 2392–2397.
[39] S.J. Wu, N. Duan, X.Y. Ma, Y. Xia, H.X. Wang, Z.P. Wang, Anal. Chim. Acta 782 (2013) 59–66.
[40] Z.G. Chen, H.L. Chen, H. Hu, M.X. Yu, F.Y. Li, Q. Zhang, Z.G. Zhou, T. Yi, C.H. Huang, J. Am. Chem. Soc. 130 (2008) 3023–3029.
[41] C.H. Liu, H. Wang, X. Li, D.P. Chen, J. Mater. Chem. 19 (2009) 3546–3553.
[42] X.H. Ji, X.N. Song, J. Li, Y.B. Bai, W.S. Yang, X.G. Peng, J. Am. Chem. Soc. 129 (2007) 13939–13948.
[43] N.R. Jana, L. Gearheart, C.J. Murphy, Adv. Mater. 13 (2011) 1389–1393.
[44] R. Elghanian, J.J. Storhoff, R.C. Mucic, R.L. Letsinger, C.A. Mirkin, Science 277 (1997) 1078–1081.
[45] C.A. Mirkin, R.L. Letsinger, R.C. Mucic, J.J. Storhoff, Nature 382 (1996) 607–609.
[46] X. Chen, H. Liu, X. Zhou, J. Hu, Nanoscale 2 (2010) 2841–2846.
[47] M. Li, X.J. Zhou, W.Q. Ding, S.W. Guo, N.Q. Wu, Biosens. Bioelectron. 41 (2013) 889–893.
[48] C.W. Liu, C.C. Huang, H.T. Chang, Anal. Chem. 81 (2009) 2383–2387.
[49] A. Ono, H. Togashi, Angew. Chem. Int. Ed. 43 (2004) 4300–4302.
[50] F. Li, L.M. Yang, M.Q. Chen, P. Li, B. Tang, Analyst 138 (2013) 461–466.
[51] I. Smirnov, R.H. Shafer, J. Mol. Biol. 296 (2000) 1–5.
[52] T. Li, S.J. Dong, E.K. Wang, J. Am. Chem. Soc. 132 (2010) 13156–13157.
[53] M. Li, X.J. Zhou, S.W. Guo, N.Q. Wu, Biosens. Bioelectron. 43 (2013) 69–74.